This manuscript has been submitted to ***Sedimentology*** and is currently under review.

Sorting of fine-grained sediment by currents: Testing the sortable silt hypothesis with laboratory experiments

Jeff Culp[a,1], Kyle Strom[a,*], Andrew Parent[b], Brian W. Romans[b]

[a] *Virginia Tech, Civil and Environmental Engineering, Blacksburg, VA USA*
[b] *Virginia Tech, Geosciences, Blacksburg, VA USA*

Abstract

Accumulations of fine sediments along continental shelf and deep-sea bathymetric contours, known as contourite drifts, form a sedimentary record that is dependent on oceanographic processes such as ocean-basin-scale circulation. A tool used to aid in interpretation of such deposits is the sortable silt (SS) hypothesis. The hypothesis suggests that the mean size of the SS (silt in the 10-63 μm size range) within a deposit is linearly related to current velocity at the time of deposition. While the hypothesis has been applied to numerous drift deposits, it has not been extensively tested. Slow deposition rates of contourite drift systems make it difficult to robustly test the hypothesis in the deep ocean, and the few laboratory studies that have been conducted have yielded inconclusive results. In this study we use laboratory flume experiments to test whether or not the mean SS in a deposit is linearly related to average current velocity; we also examine how this relationship changes as a function of distance from the inlet. Tests were conducted with 4 different sediment mixtures (pure clay, pure silt, 2:1 clay:silt and 1:1 clay:silt) and current velocities typical of deep-sea settings (5-25 cm/s). Each experiment was run with a constant supply of sediment at the flume inlet for a set amount of time. Bed samples were collected at fixed locations from the flume entrance and sized. The deposit morphology was dependent on the sediment mixture and flow conditions, but deposit grain size consistently fined downstream and coarsened with velocity. Regardless of bed morphology or source sediment mixture, the mean SS was linearly related

*Corresponding author
Email address: `strom@vt.edu` (Kyle Strom)
[1] Currently at: Dewberry, Richmond, VA

to velocity at a particular flume location across all sediment mixtures (R^2 = 0.7-0.94). The slope of the relationship increased with distance from the flume inlet. Our findings support the validity of mean sortable silt as a proxy for paleocurrent velocity.

Keywords:
sortable silt, contourite drift, advective sorting, silt, clay

---

1. Introduction

Sedimentary deposits composed of particles < 63 μm in size (i.e., mud/mudstone) make up the majority ($> 60\%$) of Earth's sedimentary record (Schieber, 1998), contain valuable archives of past environments and climate conditions (e.g., Knutz, 2008), and host important energy resources (e.g., Jarvie et al., 2007; Slatt, 2011). However, the physical processes that erode, transport, and deposit fine-grained sediment are still poorly understood compared to other sedimentary deposits (Schieber, 2011). Significant progress has been made over recent years demonstrating that clay (< 4 μm) can behave hydrodynamically similar to sand-size grains (e.g., bedload transport and associated bedform development) as a result of aggregation into larger, composite particles (up to 0.1-1 mm in size; Schieber et al., 2007); however, there has been comparably less focus on the silt fraction (4-63 μm). The "sortable silt" proxy, which was developed by the paleoceanography community to aid reconstruction of past deep-ocean current activity (**?**McCave and Hall, 2006), provides a framework to further investigate the silt range in the context of addressing the fundamental question of whether silt is sorted by bottom currents.

Bottom currents in marine environments are responsible for the erosion, transport, and deposition of fine-grained sediment. In some areas, including coastal zones, continental shelves and shallow seas, and the deep ocean, significant accumulations of muddy deposits develop over geologic timescales ($> 10^6$ yr) and, thus, represent archives of bottom-current history. For example, in the deep ocean, long-lived ocean-basin-scale boundary currents are a key component of global ocean circulation (Broecker et al., 1998) and have been linked to contourite 'drift' deposits that exceed two km in thickness and extend for 100s of km (Heezen et al., 1966; Rebesco et al., 2014). Paleoceanographers have been especially interested in reconstructing bottom-current history from contourite drift deposits because of the linkage of abyssal currents to thermohaline circulation and global climate. To aid in reconstruction, McCave et al. (1995) proposed a sedimentological proxy for changes in current velocity that relate the size of non-cohesive silt to the speed of the eroding or depositing flow. Specifically, McCave et al. (1995) hypothesized that particles within the size range of 10 to 63 μm, defined as "sortable silt" (SS), sort by size with current velocity during deposition and erosion (see McCave and Hall, 2006, for a comprehensive review). Key statistics associated with this size range that have been linked to velocity of ocean bottom currents include the mean SS, SS_{mean}, and the SS percentage, $SS\%$ (McCave and Andrews, 2019).

Despite the widespread application of SS to deep-sea sediment core samples of mostly Quaternary deposits (e.g., Kleiven et al., 2011; Thornalley et al., 2013) and some attempts at field calibration (McCave et al., 2017), the proxy remains largely untested under controlled conditions. Slow deposition rates of contourites (2-10 cm/kyr) make it difficult to robustly test the hypothesis in the deep ocean, and the limited number of laboratory studies that have been reported have yielded either inconclusive or conflicting results. Only two known studies have sought to explicitly test ideas related to the SS hypothesis. The first, Law et al. (2008), tested whether or not silt and clay beds are subject to sorting through the process of selective erosion of fine grains. Using core samples from the Gulf of Lions and a fluid shearing device known as a Gust chamber, Law et al. (2008) found that sediment samples with less than 7.5% clay were subject to sorting via selective erosion (or winnowing), but that beds with more than 7.5% clay were not susceptible to sorting. In cases with clay content greater than 7.5%, the core surface tended to fail en masse rather than grain by grain. The study highlighted the possibility of sorting by winnowing in non-cohesive beds and the importance of clay (present and abundant in the majority of deep-sea drifts) in modulating sorting, but it was unable to examine sorting under currents or in depositional environments.

Adding to the work of Law et al. (2008), Hamm and Dade (2013) used controlled laboratory experiments conducted in a recirculating, oval-track flume to examine sorting by a unidirectional current. Rather than focusing on selective erosion only, they tested the SS proxy over current velocities that allowed for both deposition and re-entrainment of previously deposited material in a current. In the experiment, they used silt-sized glass spheres (diameters between 13-44 μm) for sediment, with no clay-sized sediment added, and current velocities between 20 and 53 cm/s. In the end, Hamm and Dade (2013) reported no evidence of significant sorting of grain size within the bed as a function of current velocity. While their results did not confirm the SS hypothesis originally proposed by McCave et al. (1995), they suggested that the study was not able to make any conclusions about the appropriateness of the SS proxy under the conditions of advective down-current sorting of silt from a sediment source due to the recirculating nature of their flume.

Both of these prior studies have focused on conditions that produce re-entrainment or erosion of bed material. However, it is likely that the majority of deep-sea drift strata develops under largely depositional environments (current velocity $<$ 25 cm/s). The field studies of Ledbetter (1986) and McCave et al. (2017) suggest that size statistics in the silt range may indeed serve as a viable proxy for oceanic bottom current velocity. Yet the velocity range over which their data suggests that there is a correlation between velocity and silt size statistics is for $U < 25$ cm/s; a velocity range that has not been tested experimentally. Furthermore, if the sampled deposits develop under down-current dispersal of suspended sediment that originated from localized erosion in a benthic storm (Richardson et al., 1993), then it is possible that down-current advective transport from a source may in fact be one of the more important mechanisms of sorting (a mechanism not examined in either Law et al. (2008) or Hamm and Dade (2013).

The SS hypothesis stands as a valuable potential proxy for bottom current speed. The broad purpose of our study is to expand the conditions under which the relationship between SS size statistics and current velocity have been experimentally examined. In contrast to previous work, our laboratory experiments focus on downstream advective sorting from a source of suspended sediment under primarily depositional conditions using sediment composed of different mixtures of silt and clay. Our specific aims are to test whether or not the mean of the sortable silt within a deposit is linearly related to average current velocity, and to examine how this relationship changes as a function of distance from the sediment input location and the amount of clay present in the source suspension.

2. Methods

2.1. Approach

In this study we seek to investigate, via a flume study, (1) the functionality between the mean SS, SS_{mean}, and current velocity, U, at a particular location, and (2) how that functionality changes with the distance from the sediment input location and the initial composition of that sediment. The current velocities we are interested in correspond to those primarily observed in oceanic bottom currents, i.e., $U = 0$ to 25 cm/s (McCave et al., 2017). Velocities in this range are sufficient to move silt-sized material, but they are generally insufficient to cause large scale erosion or pull material up into suspension (McCave et al., 1995; Niño et al., 2003; Hamm et al., 2009; Hamm and Dade, 2013). Therefore, the experiments are net depositional with any sorting that occurs likely coming from selective deposition or re-entrainment of grains rather than erosion of a preexisting bed.

Laboratory studies of cohesive sediments and silts have used different flume types, e.g., traditional recirculating laboratory flumes (Einstein and Krone, 1962), annular flumes (Haralampides et al., 2003; Partheniades, 2006; Lau and Krishnappan, 1992), enclosed shear chambers (Teeter, 1997; Law et al., 2008), race-track flumes (Schieber et al., 2007; Hamm et al., 2009; Hamm and Dade, 2013; Yawar and Schieber, 2017), and non recirculating flumes (Dixit et al., 1982). Each flume type has its own strengths and weaknesses when it comes to studying the movement of sediment. A traditional recirculating flume works well for sand and gravel studies, but the high shear stress encountered in the pumps makes it less ideal for studying cohesive sediment behavior when flocculation could be an important process of consideration. In addition, deposition of fine sediment within the flume system (flume, tailbox, pipes, and headbox) makes it difficult to maintain a constant concentration at the flume inlet (Mooneyham and Strom, 2018). Annular flumes are ring-shaped channels of water that counter rotate to induce a constant shear across the bed of the flume. While an annular flume can maintain constant shear over long periods of time without passing sediment through pumps and pipes, it cannot be used to examine changes in the deposition with distanced traveled from a source because the sediment in suspension keeps getting wrapped around the same section of bed. Oval-shaped "racetrack" flumes are similar in that no pumps or pipes are involved and material is continuously moved around a closed circuit. Such systems work well for developing equilibrium conditions between deposition and erosion, but they also do not allow for examination of how the distance from the input alters the nature of the deposit. Taking these limitations into consideration, we chose to use a linear flow-through flume in which no water or sediment is recirculated back to the inlet. Our approach with the experiments is therefore similar to that of Dixit et al. (1982). While this type of flume is resource intensive, it does allow for a constant upstream concentration boundary condition and the development of spatial patterns in the deposit.

Four different sediment mixtures (pure clay, pure silt, 2:1 silt to clay and 1:1 silt to clay) were used in the experiments. In all cases, a well-mixed suspension of water and sediment was fed at a constant rate at the upstream end of the flume. Beds developed downstream with spatially varying patterns as sediment deposited from flow. The deposited bed that remained at the end of each experiment was then sampled at 1.52 m (5 ft) increments from the inlet and measured with a SediGraph 5120 particle size analyzer to allow for calculation of SS_{mean}. Current velocities for the experiment ranged from 5 to 25 cm/s.

2.2. Depositional theory

In this section we develop a simplified theory to predict the size distribution of silt in a deposit and thereby a naive assumption regarding the behavior of $SS_{mean} = SS_{mean}(x, U)$. Comparing the experimental results to the theory provides the opportunity to extend the laboratory results to larger scales if the model is found to describe the data well. The model also can be used to help inform what processes are important to consider if the experimental data deviates from the expectation set by the simplified theory.

The context of the model is that of depositional sorting in a boundary layer flow. As such, the model's foundation is provided by the one-dimensional (layer-averaged) advection-dispersion equation for suspended sediment of grain size fraction i:

$$\frac{\partial (AC_i)}{\partial t} + \frac{\partial (AUC_i)}{\partial x} = \frac{\partial}{\partial x}\left(AK_x \frac{\partial C_i}{\partial x}\right) + b\left(E_{b,i} - D_{b,i}\right) \tag{1}$$

where A is the cross sectional flow area of the current containing sediment, b is current width, C_i is the layer-averaged concentration of suspended sediment (the total concentration is $C = \sum C_i$), K_x is the dispersion coefficient, $E_{b,i}$ is an erosive flux and $D_{b,i}$ is a depositional flux for grain size fraction i across the sediment-water interface.

Assuming steady, uniform hydraulics and a rectangular or top-hat current cross-sectional area with a constant sediment input, Equation 1 simplifies to:

$$bhU\frac{\partial C_i}{\partial x} = b\left(E_{b,i} - D_{b,i}\right) \tag{2}$$

Here h is the flow thickness with the cross-sectional flow area being defined as $A = bh$. The solution of Equation 2 yields $C_i = C_i(x)$ if models for the deposition and erosion flux are specified. Typically the maximum deposition flux for grain size fraction i is taken to be $D_{b,i} = \alpha_i w_{s,i} C_{b,i}$, where $w_{s,i}$ is the settling velocity for size i and $C_{b,i}$ is the near-bed concentration of size fraction i; α_i can be thought of as the ratio of the true depositional velocity of size fraction i divided by the still water settling velocity, $w_{s,i}$. $E_{b,i}$ is often modeled as $E_{b,i} = w_{s,i}E_{s,i}$ where $E_{s,i}$ is a dimensionless erosion or entrainment velocity.

To solve Equation 2, constant values or closure equations are needed for α_i and $E_{s,i}$. When the particle diameter is less than the thickness of the viscous sublayer, the experiments of Hamm et al. (2009) on the deposition and erosion rate of silt suggest that α_i and $E_{s,i}$ are both controlled by the ratio of the viscous lift to the particle's gravitational body force. In such cases, the analytic solution for viscous lift given by Saffman (1965) for small particle Reynolds numbers yields a ratio of these two forces that is proportional to $u_*^3/(g'\nu)$; here u_* is the friction velocity and $g' = gR_s$ with R_s being the submerged specific gravity of the sediment ($R_s = 1.65$). Hamm et al. (2009) referred to this ratio as the Saffman parameter, $S \equiv u_*^3/(g'\nu)$. The analytic expression for the gravitational and lift forces are both dependent on particle diameter. However, both forces are proportional to d^3, resulting in the ratio of the forces being independent of particle size. Based on curve fitting, Hamm et al. (2009) found that their experimental data was best described with:

$$\alpha = 1 - S \tag{3}$$

$$E_s = S^{5/2} \tag{4}$$

For our naive model, we adopt Equations 3 and 4, resulting in size-independent α_i and $E_{s,i}$ values. Assuming a well-mixed condition for suspended sediment over the thickness of the turbid boundary layer ($C_{b,i} = C_i$), the deposition and entrainment fluxes become:

$$D_{b,i} = \alpha w_{s,i} C_i \tag{5}$$

$$E_{b,i} = w_{s,i} E_s \tag{6}$$

Therefore, the net rate of deposition to, or accumulation in, the bed of sediment of size fraction i is:

$$D_{b,i} - E_{b,i} = w_{s,i}(\alpha C_i - E_s) \tag{7}$$

Using the rate of accumulation, the total fraction of the bed material of size i can be defined as:

$$f_{b,i} = \frac{w_{s,i}(\alpha C_i - E_s)}{\sum w_{s,i}(\alpha C_i - E_s)} \tag{8}$$

Values of $f_{b,i}$ as a function of distance are what one needs to develop predictions for the spatial arrangement of SS_{mean} in the flume or a boundary current. $f_{b,i} = f_{b,i}(x)$ can be obtained from the solution of Equation 2 using Equations 5 and 6 for the exchange rates of material at the water-sediment interface. The result is:

$$C_i = \left(C_{i,0} - \frac{E_s}{\alpha} \right) e^{-\frac{\alpha w_{s,i}}{hU} x} + \frac{E_s}{\alpha} \tag{9}$$

The ratio of $hU/(\alpha w_{s,i})$ can be thought of as the horizontal advective length scale for sediment of size i, $L_i = hU/(\alpha w_{s,i})$. Therefore Equation 9 can also be written as:

$$C_i = \left(C_{i,0} - \frac{E_s}{\alpha} \right) e^{-\frac{x}{L_i}} + \frac{E_s}{\alpha} \tag{10}$$

When coupled with a settling velocity equation (e.g., Ferguson and Church, 2004), the model (Eqs. 8 and 9 or 10) predicts the silt size distribution in the bed as a function of the distance from the input, x, the current velocity, U, the current thickness, h, the size distribution of the source material, and the Saffman parameter (or u_*, which we link to U). An implicit assumption embedded in the model is that deposited material is immobile; that is, the model does not account for bed load transport.

We used this naive model to examine $f_{b,i} = f_{b,i}(x, U)$ and the resulting $SS_{mean} = SS_{mean}(x, U)$ over the x and U values expected in our experiments (Fig. 1). The exact definition of SS_{mean} is given below in the Section 2.5. To make the calculations, we used (1) a synthetic initial SS size distribution based on our input sediment, and (2) the $u_* = u_*(U)$ relation from our experiments. The synthetic SS distribution reasonably mimics the average SS size distribution used in the experiments and was developed assuming the natural log transformed grain sizes are normally distributed with a mean of $\theta_m = 3.2$ (24.5 μm) and a standard deviation, $\sigma = 0.8$ ($\theta_m - \sigma = 11$ μm and $\theta_m + \sigma = 54.5$ μm). For context, u_* values from our experiments produced Saffman numbers between 0.002 to 0.15, and therefore α values ranging from 1 to 0.85 with $E_s \approx 0$.

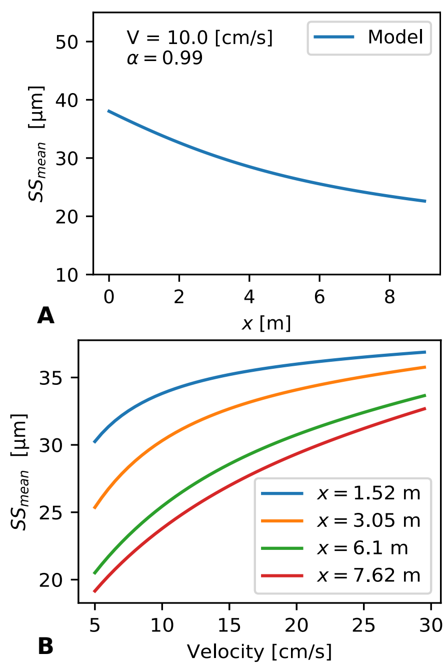

Figure 1: Simple naive model for $SS_{mean} = SS_{mean}(x, U)$ based on Eqs 9 and 2

The model predicts a decrease in SS_{mean} with distance from the inlet or source of suspended sediment, x, as one would expect for general downstream fining under advective sorting (Fig. 1A). Increases in either h or U results in coarsening at a given location (Eq. 9) due to the increase in the advective length scale, L_i; doubling either h or U produces a doubling of L_i. For fixed x and h (that is, at a station), SS_{mean} increases with U (Fig. 1B). The model predicts that the relationship between SS_{mean} and U becomes increasingly closer to linear with an increasing distance from the input. In addition, the slope of the SS_{mean} and U relation also increases with distance (Fig. 1B). This implies that the suggested linear relationship between an average silt size Ledbetter (1986) or SS_{mean} McCave et al. (2017) applies best to the model output at longer distances from the sediment input location.

2.3. Experimental equipment and general methodology

All experiments were conducted in a 18 cm wide, 9.14 m long, tilting acrylic flow-through flume (Fig. 2). The inflow for the system is controlled with a constant head tank and valve on the inflow line. Water from the tank is discharged to a mixing tank, where sediment is added via a calibrated AccuRate dry material feeder, and then to the flume headbox. From there the suspension passes through flow straighteners, down the length of the channel, and into a settling basin before being discharged to the drain. Uniform flow is maintained over the length of the channel through adjustment of the channel slope and a series of removable vertical bars at the outlet that provide upstream facing normal force for the flow. The maximum amount of flow that can be put through the system is dependent on the volume in the storage tank that pumps to the constant head tank, the volume flow rate of water that can be added to the storage tank, and the capacity of the drain line in the laboratory. Taken together, the maximum flow velocity that can be sustained with the system is 28 cm/s at a flow depth of 3.4 cm for 2 hours, which yields a maximum functional discharge of 1.7 L/s ($\approx$ 27 gpm).

Other equipment used in the experiments included an overhead camera (Cannon 80D) attached to a sliding rail and Campbell Scientific Optical Backscatter Senors (OBS) 3+ probes (Fig. 2). The camera was used during the experiments to observe, when possible, the development and movement of the bed through video and time-lapse photography. The camera was also used to develop a mosaic of the entire bed after water

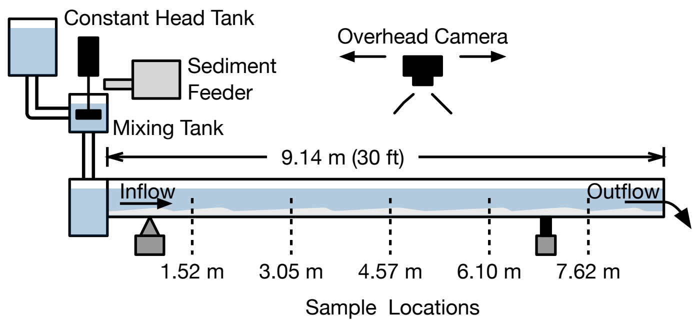

Figure 2: Experimental Setup.

had been drained from the flume at the completion of each run. The OBSs sensors were installed at the up and downstream ends of the flumes for a subset of runs to monitor concentration. These were calibrated beforehand using each of the sediment mixtures over a large range of concentrations. All regressions for the OBSs were done with 18 or more points, and R^2 values for each exceeded 0.99.

Each experiment proceeded by setting the discharge to the desired rate, checking for the development of uniform flow in the channel and adjusting the number of bars at the flume exit as needed, followed by engagement of the sediment feeder. All experiments were run for a duration of 2 hours; through preliminary experiments 2 hours was determined to be a sufficient amount of time to accumulate enough sediment in the bed for sampling. The conditions used in the experimental matrix are given below following a discussion on results from a set of preliminary tests.

Flow velocity, U, was calculated for each run using the measured volumetric discharge, Q, the measured flow depth, h, and known flume width, w, as $U = Q/(hw)$. Shear velocity, u_*, values for each case were obtained by solving the smooth-wall Keulegan resistance equation,

$$\frac{U}{u_*} = \frac{1}{\kappa} \ln\left(\frac{hu_*}{\nu}\right) 5.5 - \frac{1}{\kappa} \tag{11}$$

where, $\kappa = 0.4$ is the von Karman constant and ν is the kinematic viscosity of the water. The bed shear stress, τ_B is related, by the definition of the friction velocity, as $\tau_B = \rho u_*^2$.

2.4. *Deposit sampling and grain-size measurement*

The sediment used in the experiments included pure silica silt sourced from US Silica under the name SIL-CO-SIL, kaolinite supplied by Georgia Kaolinite, and a 100% non-treated sodium bentonite of the name Aquagel Gold Seal. Four mixtures were tested at varying flow velocities: 100% silica silt, 5:4:1 silica silt:kaolinite:bentonite, 5:8:2 silica silt:kaolinite:bentonite, and 4:1 kaolinite:bentonite. These sediment mixtures will hereafter be referred to as pure silt, silt to clay 1:1, silt to clay 1:2, and pure clay respectively. These clay:silt ratios resemble those found in muddy and silty contourites (Rebesco et al., 2014; McCave and Hall, 2006) as well as those tested in flocculation experiments that found silt to entrain into flocs in a depositional environment (Tran and Strom, 2017). The clay in the experiments did form aggregates, but these aggregates were small and more compact than the loosely bound flocs of Tran and Strom (2017). Grain size distributions of the input sediment mixtures used for each experiment can be seen in Figure 3.

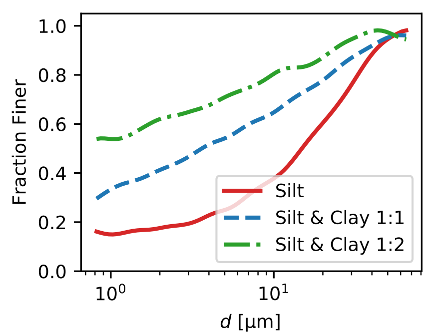

Figure 3: Initial grain size distributions for the three mixtures that included silt.

Bed samples were collected after the water had mostly drained from the flume after each 2-hr run at five stations at distances of 1.52 m (5 ft), 3.05 m (10 ft), 4.57 m (15 ft), 6.10 m (20 ft), and 7.62 m (25 ft) from the inlet (Fig. 2). To ensure the capture of all of the fine sediment, the samples were collected using a large syringe over a 5 cm x 5 cm patch of bed (or an area large enough to sample a minimum of 1 g of sediment by dry weight). Each sample contained both sediment and water. These samples were stored in labeled vials for sizing at a later time and the syringe was flushed with clean water several times between each sample to ensure that samples from a given site were not contaminated with remnant grains from a different location or experimental run.

The grain size distribution of each bed sample was measured using a Micromeritics SediGraph 5120. The SediGraph is a reliable instrument for measuring the grain size distribution of fine-grained sediments (e.g., Bianchi et al., 1999) and has been used extensively for SS proxy applications. The SediGraph calculates grain size distribution using x-rays to measure sediment concentration and settling velocity, which is then used to compute grain size using Stokes' Law:

$$d = \left(\frac{18 w_s \nu}{g'}\right)^{1/2} \tag{12}$$

Once bed samples were collected, water was decanted and bulk sediment was dried for 48 hr. Once samples were sufficiently dried, a 1.0 g split was separated for analysis in the SediGraph. The split was dispersed in 65 mL of analysis fluid: ultra-pure (18.2 Ω m resistivity) water for pure silt samples and 0.5% tetrasodium pyrophosphate (TSPP) ultra-pure water for samples containing clay, to reduce particle flocculation during analysis. Samples dispersed in TSPP underwent a 15 min ultrasonic bath to further eliminate flocculation of the sample.

2.5. Calculation of the mean sortable silt

SS_{mean} was calculated from the natural log transformed bin sizes, $\theta_i = \ln(d_i)$ where d_i is the percent finer than bin edge in microns used in the process of measuring and quantifying the total grain size distribution of a sample (e.g. a SediGraph output). SS_{mean} is defined as:

$$SS_{mean} = e^{\theta_m} \tag{13}$$

with θ_m defined as,

$$\theta_m = \sum_{i=1}^{n} \overline{\theta_i} f_{ss,i} \tag{14}$$

where $\overline{\theta_i}$ is equivalent to the "natural log of the bin's geometric mid-point diameters", $\overline{\theta_i} = (\theta_i + \theta_{i+1})/2$ (McCave and Andrews, 2019), and $f_{ss,i}$ is the fraction of material associated with the SS size range (10 to 63 μm) in bin i. $i = 1$ is associated with the bin whose lower edge is 10 μm; $i = n$ is associated with the bin whose upper edge is 63 μm: $f_{ss,i} = p_i / \sum_{i=1}^{i=n} p_i$.

2.6. Defining the experimental conditions

A series of preliminary experiments were run to determine the general repeatability of the methods and the influence of inlet sediment concentration, flow depth, and experimental runtime on the SS_{mean} in the deposit for the purpose of defining the final experimental conditions. Repeat 2 hr experiments, even at different concentrations, generally showed less than ± 1 μm variation between any individual SS_{mean} statistic at a given sampling location. This suggests that the experimental methods show little variation in SS_{mean} from run to run. The one exception to this was that up to 1.4 μm variation was observed at the most distal location (Fig. 4A). The fact that the variability between SS_{mean} at a given location under different inlet concentrations ($C \approx 500$ and 1000 mg/L) was also in the same variation range indicates that the deposit grain size distribution is not dependent on the inlet concentration. Inlet concentration does significantly influence the deposition rate, but it does not fundamentally change the size distribution in the deposit. This result is advantageous because it allows for running experiments at concentrations higher than would be expected in a natural boundary current to speed up time without altering the size distribution in the deposit. It also means that variations in concentration at the inlet should not impact the results.

We also examined the role of flow depth, h, on the deposit grain size distribution and resulting SS statistics (Fig. 4B). Unlike concentration, changes in flow depth do produce significant differences in SS_{mean} at a given distance downstream of the input all else being constant (e.g. constant velocity and input sediment size characteristics). This is to be expected given the dependence of $C_i = C_i(x)$ on the ratio $\alpha w_{s,i}/(hU)$ (Eq. 9). In the simple depositional model, h has as significant of an influence on the concentration profile as U. In general, increasing flow depth coarsens the deposit at a given location due to the increase in the advection length scale of a given particle size $L_i = hU/(\alpha_i w_{s,i})$ (Fig. 4B). Because we are here interested in the relationship of $SS_{mean} = SS_{mean}(x, U)$, we held depth constant at $h = 3.4$ cm in all other experiments.

If particles that deposit from the current to the bed do not move, then the grain size distributions in the beds will be independent of experimental duration. However, in our experiments, some of the deposited particles did move as bed load, and the downstream

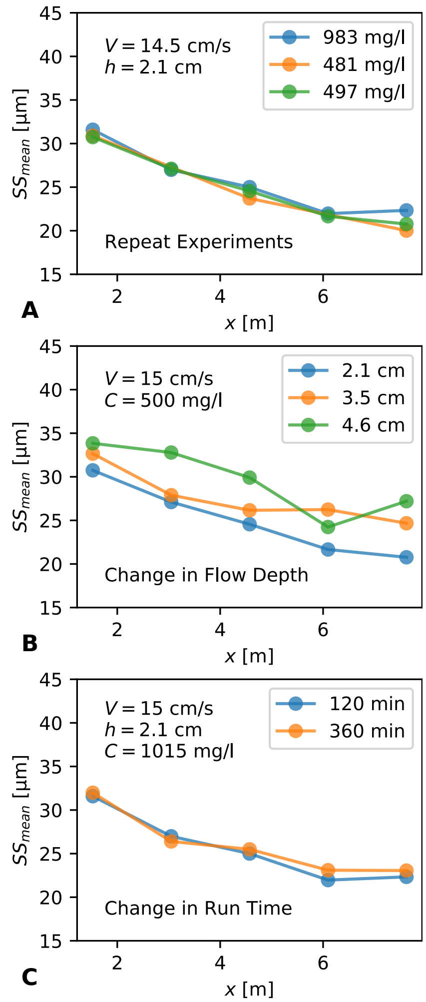

Figure 4: The distribution of SS_{mean} down channel for the preliminary runs. (A) repeat experiments no change in experimental conditions except the inlet concentration, (B) changes in flow depth, h, only, and (C) changes in experimental runtime.

movement intensified with increasing velocity. The presence of bed load suggests that the size of the sediment in the beds at a given distance down channel could change with the total runtime of the experiment. We tested the sensitivity of the measured SS_{mean} to variations in experimental run time by comparing results between a standard experimental run time of 2 hr to an experiment with a run time of 6 hr (Fig. 4C). The differences in SS_{mean} between these two experiments at the three upstream sampling locations all fell within the range of experimental variability. However, slight coarsening of SS_{mean} (≈ 1 μm) at the two most distal locations was observed (Fig. 4C). We attribute this to downstream transport via bed load motion of larger grains sizes.

Given that experimental run time could impact the distribution of SS, we fixed the run time for all experiments at 2 hr and varied the inlet concentration to ensure that enough sediment deposited during the 2 hr to be sampled and sized with the SediGraph. Flow depth was fixed at 3.4 cm for all runs, and velocity was varied from 5 to 25 cm/s (Table 1). Taken together, these conditions and procedures allow us to isolate the link between SS_{mean}, flow velocity, and distance from the input for each of the four sediment mixtures.

Sediment	Inlet Concentration, C_0 [mg/L]	Velocity, U [cm/s]
Pure Silt	374-1660	5, 10, 15, 20, 25
Pure Clay	482-2070	5, 10, 15, 20, 25
Clay & Silt (1:1 ratio)	328-1654	5, 10, 15, 20, 25
Clay & Silt (2:1 ratio)	393-1871	5, 10, 15, 20, 25

Table 1: Experimental Matrix

3. Results

3.1. Transport conditions

Before describing the bed morphology or $SS_{mean} = SS_{mean}(x, U)$ results, we here present key hydraulic and sediment transport parameters associated with each of the five experimental velocities for the purpose of contextualizing the conditions. The flow parameters presented are: the shear velocity, the bed shear stress, the thickness of the initial viscous sublayer, $\delta = 5\nu/u_*$, and the Saffman parameter, S. Two other sediment transport ratios are also provided for silt sizes 10, 30, and 60 μm. The two ratios are u_*/w_s, a measure of how well mixed particles in suspension are over the vertical, and τ^*/τ^*_{cr}, a measure of particle mobility or transport intensity for those particles that make it to the bed. For the transport intensity parameter, τ^* is the dimensionless bed shear stress ($\tau^* = u_*^2/u_g^2$) and τ^*_{cr} is the value of the dimensionless shear stress where significant bed load motion occurs. Here the τ^*_{cr} threshold was calculated as $\tau^*_{cr} = [0.22Ga^{-0.6} + 0.06\exp(-17.77Ga^{-0.6})]/2$ where Ga is the Galileo number, $Ga = u_g d/\nu$ (a type of particle Reynolds number), and u_g is the particle velocity scale associated with the submerged gravitational body force, $u_g = \sqrt{g'd}$ (García, 2008). The equation for τ^*_{cr} yields the classic Shields curve divided by 2. This reduced Shields threshold was chosen since it predicted motion for cases where $U \geq 15$ cm/s, which is in line with our observations in this study. All of the contextual parameter and ratio values are given in Table 2.

U	u_*	τ_B	δ	S	u_*/w_s			τ^*/τ^*_{cr}		
[cm/s]	[m/s]	[Pa]	[μm]	[-]	$d_{10\mu m}$	$d_{30\mu m}$	$d_{60\mu m}$	$d_{10\mu m}$	$d_{30\mu m}$	$d_{60\mu m}$
5	0.003	0.01	1632	0.002	49.4	5.6	1.5	0.2	0.2	0.2
10	0.006	0.04	930	0.012	86.8	9.8	2.6	0.6	0.5	0.5
15	0.009	0.08	641	0.038	125.8	14.3	3.7	1.2	1.1	1.0
20	0.012	0.13	491	0.085	164.3	18.6	4.9	2.0	1.8	1.7
25	0.014	0.19	413	0.143	195.6	22.2	5.8	2.9	2.6	2.4

Table 2: Conditions at a given flow velocity. δ is the thickness of the viscous sublayer. Values of u_*/w_s and τ^*/τ^*_{cr} are given for representative grain sizes of 10, 30, and 60 μm.

Values of u_*/w_s indicate transport in the downstream direction being dominated by suspended load, $u_*/w_s > 1$, and, at least for the $d = 10$ and 30 μm cases, being fairly well mixed over the vertical, $u_*/w_s > 6$; which is equivalent to a Rouse number of $Z_R = w_s/(\kappa u_*) < 0.4$ (García, 2008). Nevertheless, all runs except for the case of $U = 25$ cm/s with pure clay experienced deposition and the development of a bed that could be sampled at at least two locations in the flume.

In all runs, the thickness of the viscous sublayer exceeded the diameter of the silt in the mixture by a factor of roughly 10 (i.e., $\delta > 400$ μm). This suggests that any sediment that made it to the boundary would be submerged in the region of flow dominated by viscous effects. In such cases, the likelihood of re-entrainment of particles from the wall region can be quantified with S (Saffman, 1965; Hamm et al., 2009), with (Saffman, 1965) proposing that a value of $S = 0.65$ is needed for the viscous lift forces to overcome the gravitational forces on a particle. With our highest value being ≈ 0.15 it can be expected that most of the particles that make it to the bed will likely remain in the near bed region rather than being resuspended up into the flow.

While the Saffman values suggest that experimental conditions are in line with a net depositional setting for silt, it is still possible for particles on the bed to move in the downstream direction as bed load. The ratio of τ^*/τ^*_{cr} provides a measure of the flows ability to move particles on the bed with values greater than 1 suggesting motion. In all experiments with silt, we found the onset of bed load to be well captured by this ratio. For runs with $U < 15$ cm/s, the bed that developed was largely immobile and topographically featureless. However, for all runs containing silt in the input sediment and $U \geq 15$ cm/s, active bed load occurred throughout the experiment and led to the development of migrating bedforms.

3.2. Bed morphology

The deposit thickness, morphology, and grain size all varied spatially down the flume and with flow velocity. A constant spatial trend in all cases was that the deposit thickness decreased in the downstream direction. The bed morphology transitioned downstream from a flat deposit with a few moving particles in the surface layer, to migrating 2D ripples, and then to migrating barchan shaped 3D ripples. This pattern was present both downstream in a given experiment for cases with $U \geq 15$ cm/s and the presence of silt, and with increases in velocity from experiment to experiment at a given station. Both trends in morphology are interpreted as an outcome of a reduction in the amount of silt in the bed load layer with distance from the inlet and with increased velocity at a station. Input material also influenced the type and size of bedforms present. Increases in clay content moved the transition from a flat bed to 2D ripples, or from 2D ripples to barchan ripples, farther downstream (Figures 5-9).

At a flow velocity of 5 cm/s (Fig. 5), no bedforms were observed with any of the four inlet sediment mixtures. Instead, deposition resulted in a smooth, uniform bed throughout the length of the flume. At a flow velocity of 10 cm/s (Fig. 6), bedforms are minimal with some small ($<$ 1 cm wavelength) 2D ripples being apparent in the pure silt runs, but no true ripples forming in any run with clay.

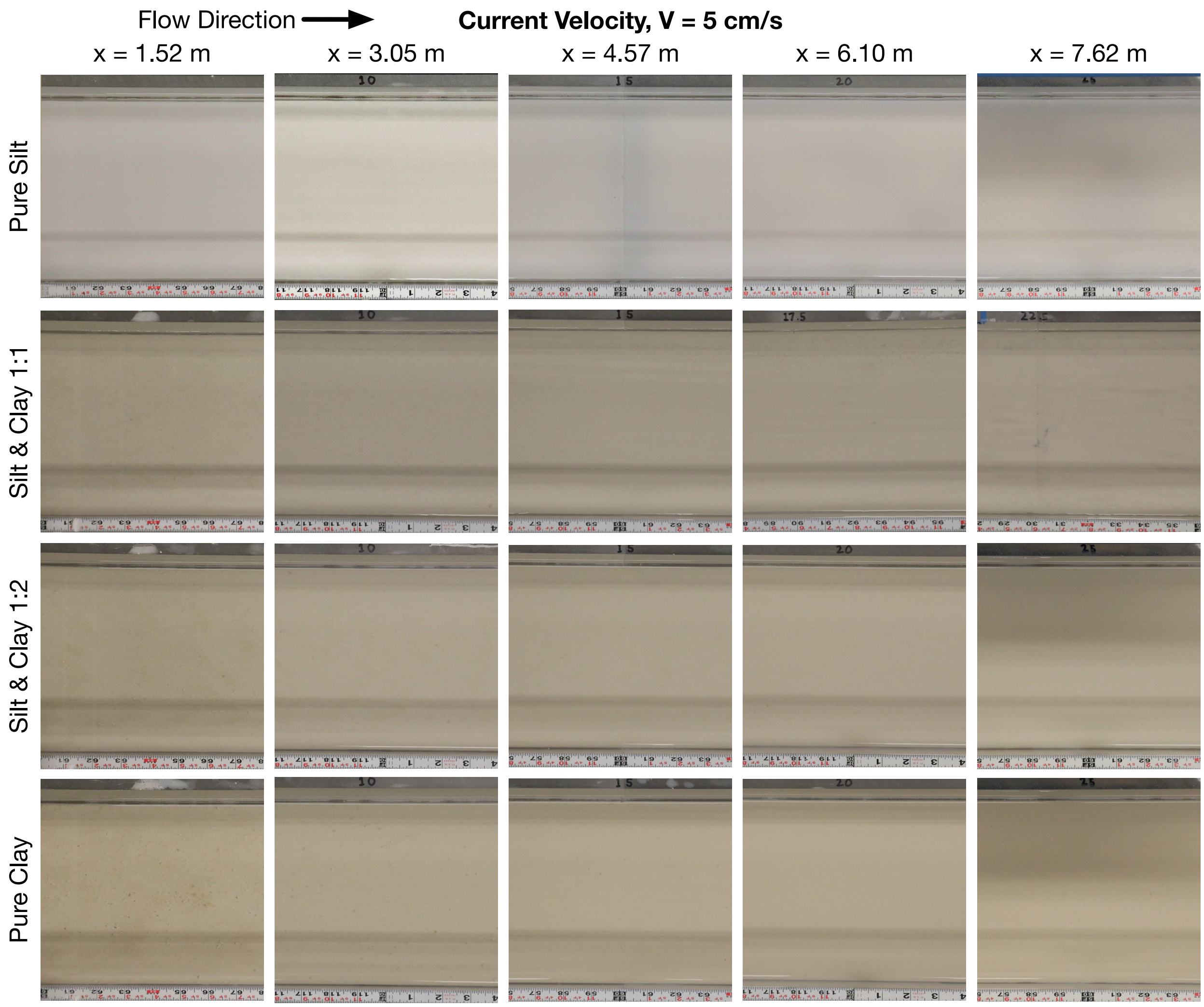

Figure 5: Images of the bed at the end of each of the $U = 5$ cm/s runs. x is the distance downstream from the inlet.

At $U = 15$ cm/s (Fig. 7), 1-2 mm tall ripples were present at the first three sampling locations in all experiments containing silt; ripples were not present in the pure clay experiment. The pure silt experiment saw a continuation of these ripples to the end of the flume, while the experiment with clay saw the ripples transition into barchan ripples around 6.4 m for the 1:1 experiment, and around 5.5 m for the 1:2 experiment.

At $U = 20$ cm/s, pure silt beds transitioned from 2D ripples to barchans moving downstream (Fig. 8). A similar pattern occurred for the clay and silt experiments, with the structures becoming more disorganized as clay content increased. Pure clay resulted in no bedforms with only a few bare patches in the bed followed downstream by a zone

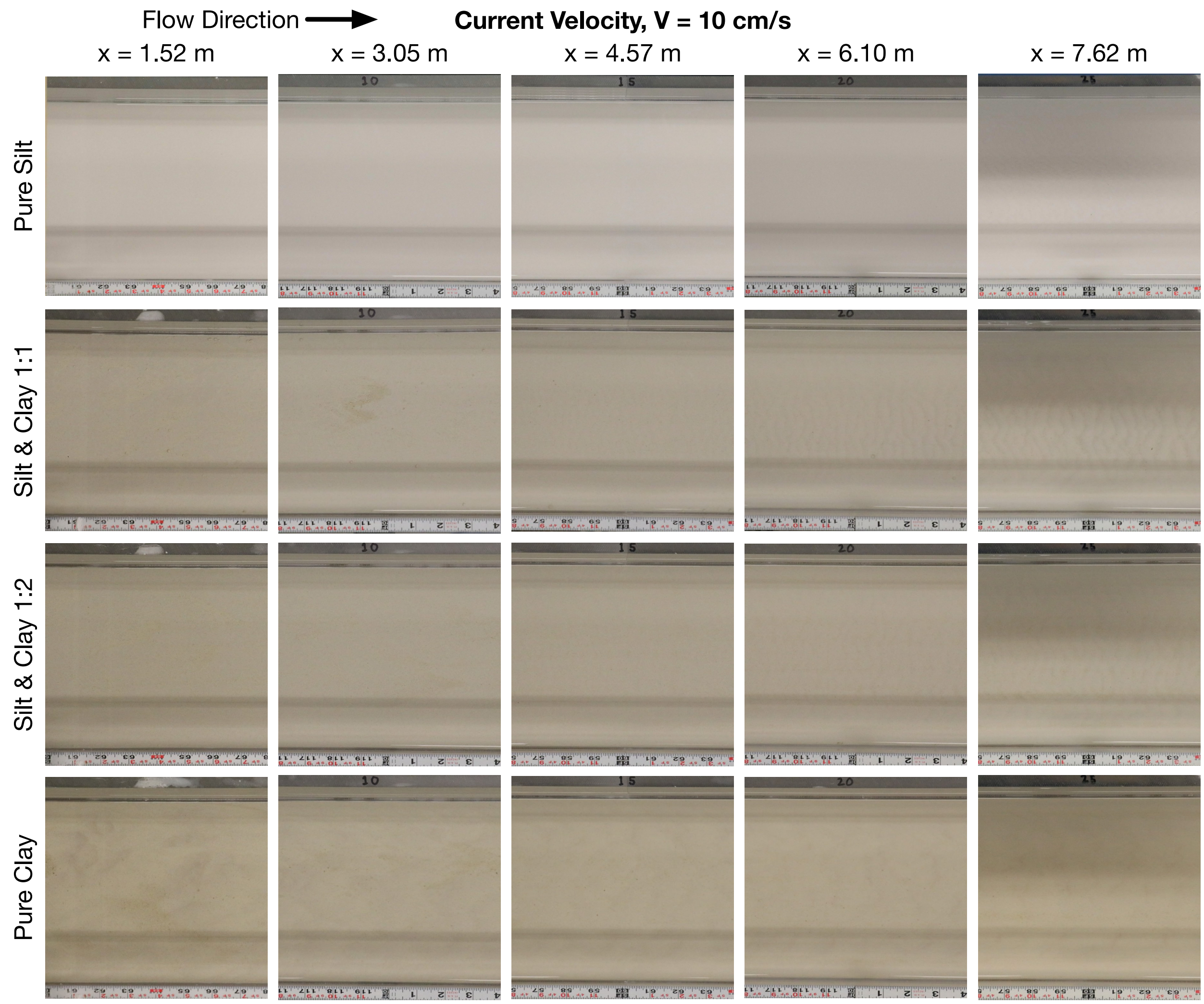

Figure 6: Images of the bed at the end of each of the $U = 10$ cm/s runs. x is the distance downstream from the inlet.

of no net accumulation of sediment. Bedload did occur in the form of what have been called floccule streamers (Schieber et al., 2007) in the zone of no net accumulation (Fig. 8, lower right). The streamers convey sediment parallel to the flow direction within low-speed streaks and where visually evident in all experiments. Increasing velocity to 25 cm/s (Fig. 9) resulted in an increase in height of the pure silt barchans (up to 8 mm, $h/h_{\text{bedform}} = 4.25$). Bedforms in the clay and silt mixtures became increasingly sparse. Large clay aggregates, likely an artifact of the mixing process, were also mobile at this velocity and were able to move as bed load down the flume, some of which deposited in the stoss and lee sided of the ripples. A thin deposit of these clumps was also observed

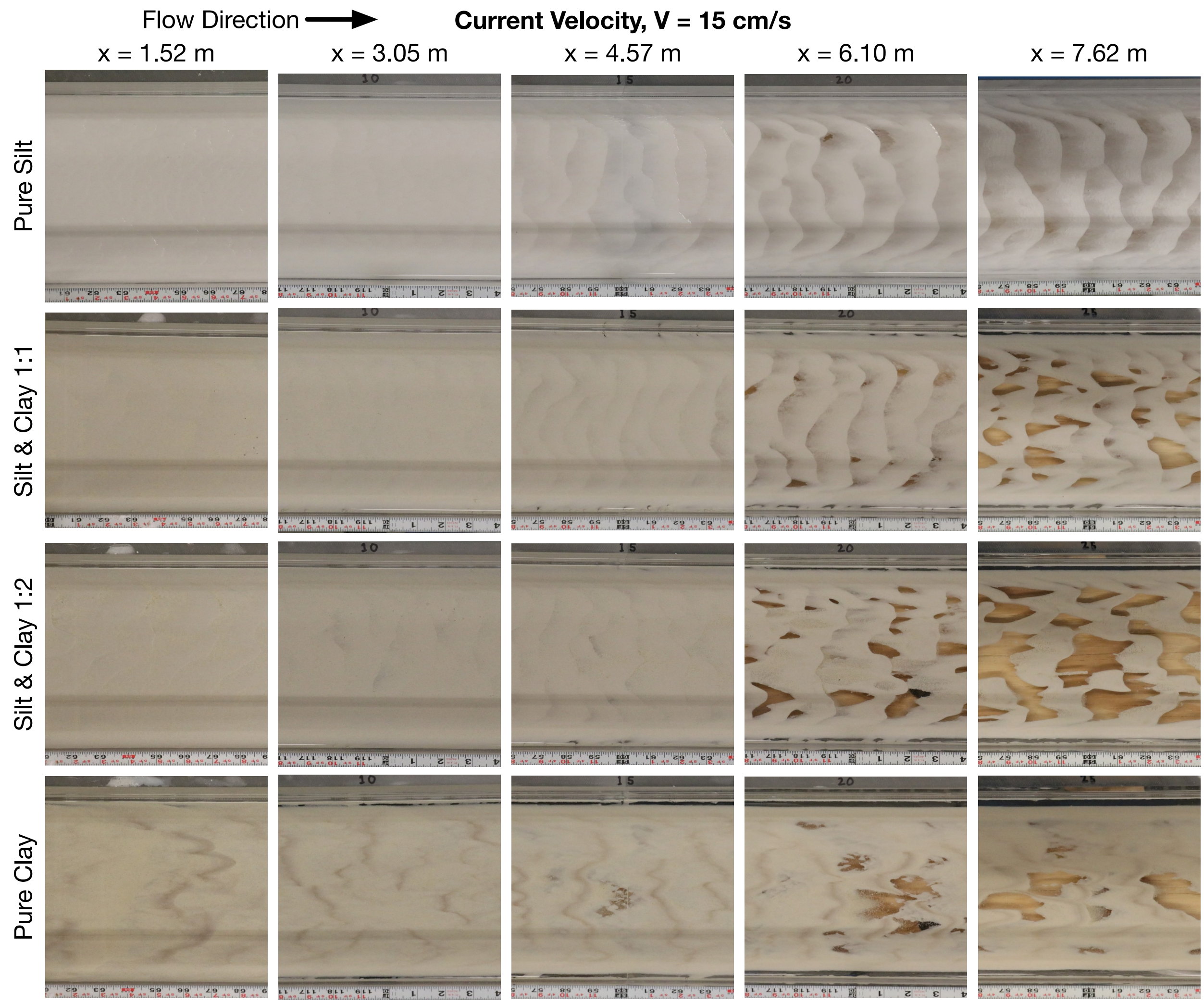

Figure 7: Images of the bed at the end of each of the $U = 15$ cm/s runs. x is the distance downstream from the inlet.

from 0-3.8 m along the flume. The experiment with pure clay did contain bed load transport but yielded no net deposition.

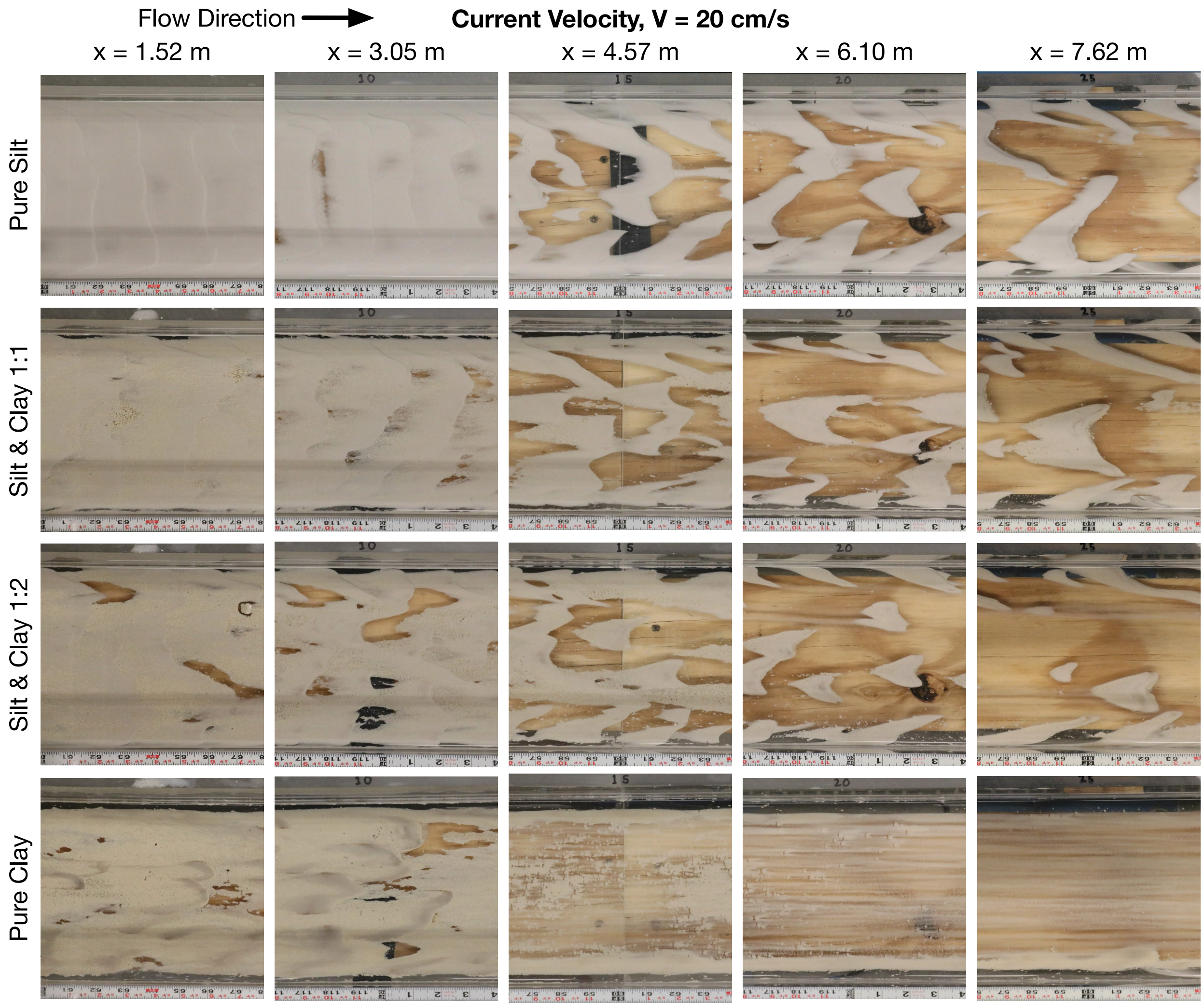

Figure 8: Images of the bed at the end of each of the $U = 20$ cm/s runs. x is the distance downstream from the inlet.

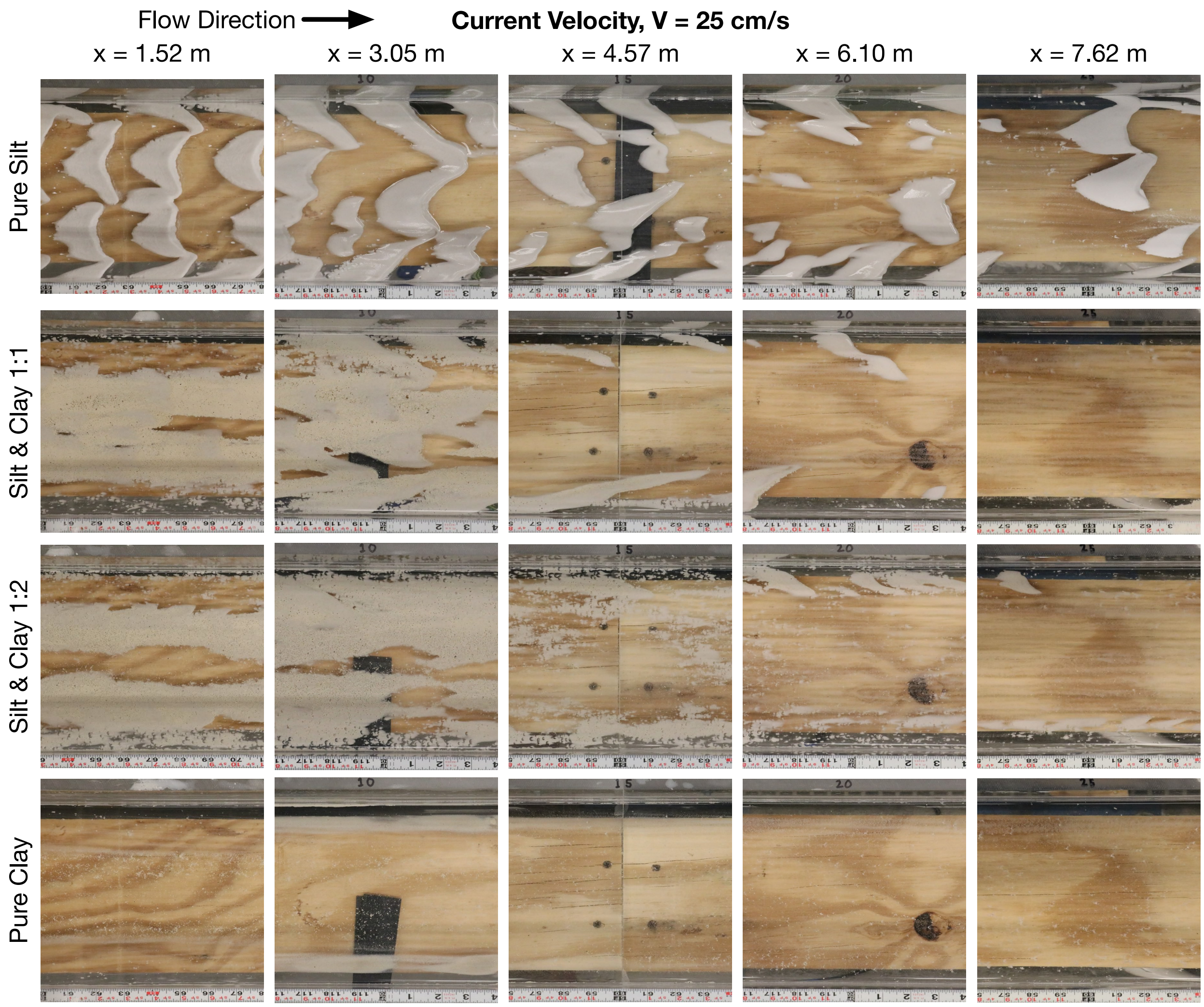

Figure 9: Images of the bed at the end of each of the $U = 25$ cm/s runs. x is the distance downstream from the inlet.

3.3. *Downstream patterns in deposit grain size*

All of the experiments using silt, regardless of the amount or type of clay added, exhibited some degree of systematic downstream fining of the SS fraction in the bed (Fig. 10). Downstream fining was stronger (more change in the bed size distribution for each step in distance downstream from the inlet) for the lower velocities than it was for higher velocity (Fig. 10). In fact, for some of the 25 cm/s runs, little change was observed in the deposit grain size distribution. This result could be interpreted as the system either needing longer distances to observe the fining or the system pushing more towards an equilibrium state between deposition and re-entrainment as velocities increase.

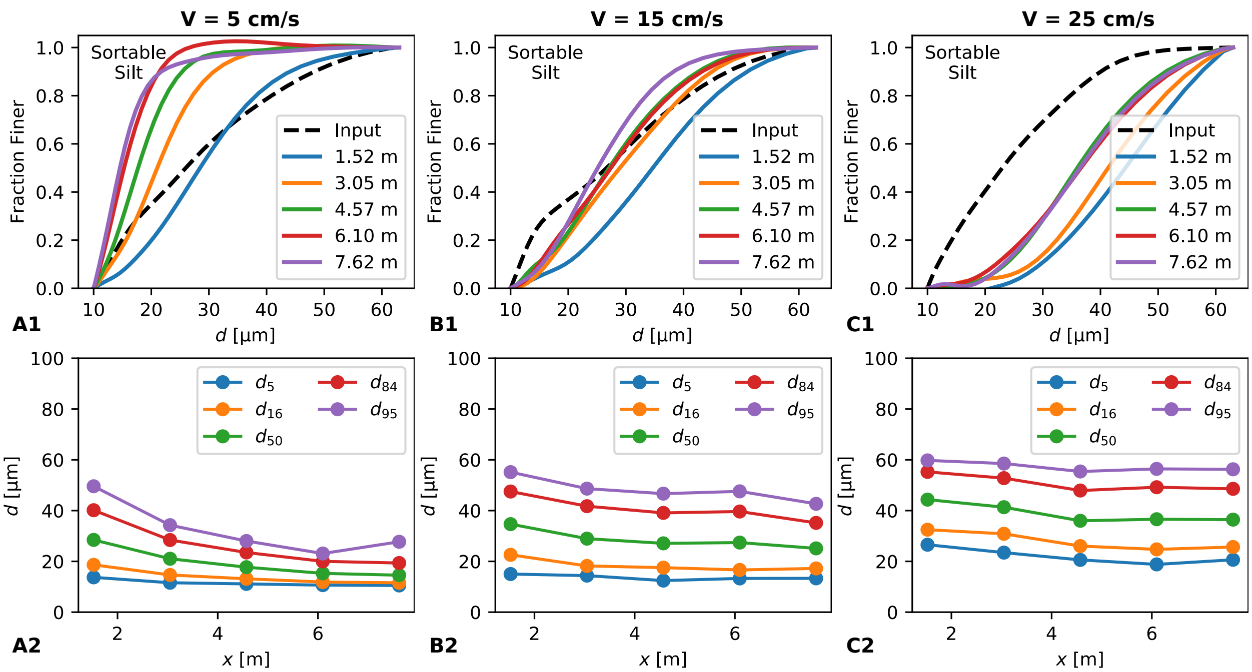

Figure 10: Downstream trends in the distribution of the sortable silt fraction for (A) $U = 5$ cm/s, (B) $U = 15$ cm/s, and (C) $U = 25$ cm/s; all plots are for runs with Pure Silt. At all velocities, the top row shows the cumulative distributions of the SS fraction and the bottom row shows the distribution statistics as a function of distance down channel from the inlet.

The size distribution data in Figure 10 also shows that the distribution of SS at a given station coarsens with current velocity. This can be observed by comparing the cumulative distribution curves at $x = 4.57$ m in the top row of the figure for velocities of 5, 15, and 25 cm/s. Because the conditions are overall net depositional ($E_s \approx 0$), the coarsening with the increase in velocity can be interpreted as the outcome of an increase in the advective length scale, L_i, (Eq. 10).

3.4. The relationship between sortable silt and current velocity at a station

SS_{mean} was calculated following the method described in Section 2.5 for every bed sample for which silt was present in the input sediment (i.e., for all runs except the pure clay runs). The range of SS_{mean} across all experiments and station locations was 15 to 45 μm; a reasonably large range considering that the SS size range is 10 to 62 μm. SS_{mean} systematically decreases progressing from the flume entrance to exit following a trend similar to the d_{50} of the SS fraction (Fig. 10).

All SS_{mean} data were grouped by station and plotted against current velocity to examine the relationship between SS_{mean} and U (Fig. 11). We performed linear regression with SS_{mean} as the scalar response and U as the explanatory variable at each station. We performed the regression for data for each sediment type independently and also for a combined dataset using SS_{mean} values from all three sediment mixtures. The fit equations for the combined dataset are shown in Figure 11; the coefficients and R^2 values for all regressions are given in Table 3. Of the four sets of regression coefficients, we have chosen the ones obtained from the combined dataset (i.e., Fig. 11 and the "All" rows in Table 3) to be the most significant since they were developed with the largest number of data points. For these regressions, R^2 ranges from 0.7 to 0.94 (Table 3).

Three trends are evident in the regression output. The first is that the data tend to be better described by linear regression as the distance from the flume inlet increases (Fig. 11). The second and third are that the slope of the fit line increases with distance from the inlet (from 0.54 to 0.8) and the intercept decreases (from 23.8 to 13.2).

While not shown in the figures or tables, we also performed a regression between SS_{mean} and the shear velocity, u_*. For our particular set of data, no predictive power was gained by using u_* instead of U. For this reason, and because the classic SS hypothesis relates SS_{mean} and velocity, we focus the discussion on the relationship between SS_{mean} and velocity rather than shear velocity or bed shear stress.

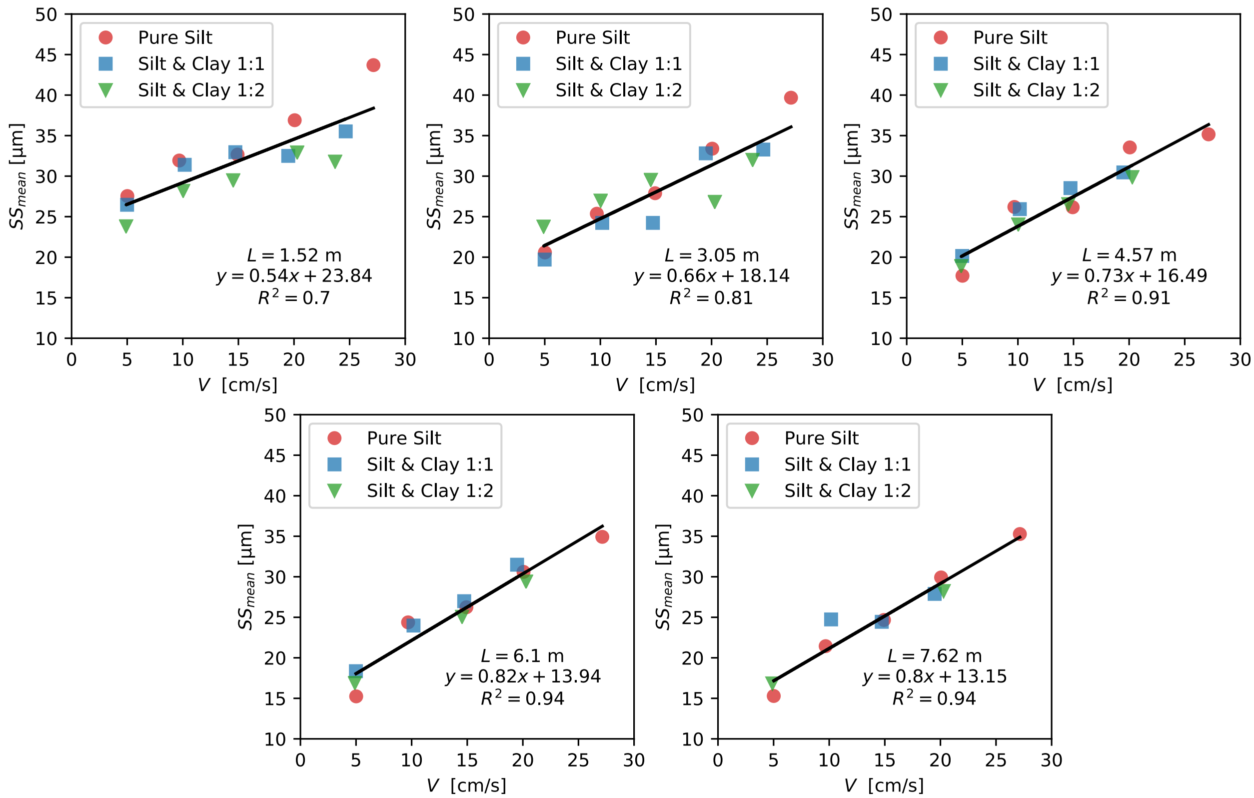

Figure 11: Regression between SS_{mean} and current velocity at each of the five sampling locations. L is the distance between the sediment input location and the sample location.

Sediment	Station, L [m]	Slope [μm-s/cm]	Intercept [μm]	R^2
Pure Silt	1.52	0.69	24.0	0.96
Pure Silt	3.05	0.85	16.4	0.99
Pure Silt	4.57	0.76	16.1	0.89
Pure Silt	6.10	0.82	13.6	0.93
Pure Silt	7.62	0.88	11.8	0.99
Silt & Clay 1:1	1.52	0.40	25.9	0.84
Silt & Clay 1:1	3.05	0.73	16.0	0.90
Silt & Clay 1:1	4.57	0.70	17.6	0.94
Silt & Clay 1:1	6.10	0.89	14.3	0.99
Silt & Clay 1:1	7.62	0.34	20.6	0.69
Silt & Clay 1:2	1.52	0.44	22.8	0.88
Silt & Clay 1:2	3.05	0.33	23.0	0.64
Silt & Clay 1:2	4.57	0.70	16.2	0.98
Silt & Clay 1:2	6.10	0.82	13.0	1.00
Silt & Clay 1:2	7.62	0.74	13.2	1.00
All	1.52	0.54	23.8	0.70
All	3.05	0.66	18.1	0.81
All	4.57	0.73	16.5	0.91
All	6.10	0.82	13.9	0.94
All	7.62	0.80	13.2	0.94

Table 3: Linear regression coefficients for $SS_{mean} = SS_{mean}(U)$. Regression slope and intercept values are given for individual sediment times (e.g., Pure Silt) and for the combination of all data from different sediment input (All). R^2 values of 1 indicate conditions were only two points were available due to the lack of deposition in some silt and clay runs.

4. Discussion

4.1. Comparison with field and other laboratory data

A primary outcome of the study is the experimental verification that silt does depositionally sort as a function of velocity over the range of $U = 5$ to 25 cm/s. We also find grain size sorting is dependent on the distance from the flume inlet to the sample location and the flow depth. Furthermore, under our experimental conditions, SS_{mean} appears to be linearly related to the average current velocity as originally proposed for the entire silt fraction by Ledbetter (1986) and later by McCave et al. (2017) for the SS fraction.

The studies of Ledbetter (1986) and McCave et al. (2017) provide the only known field data examining the relationship between the mean silt (Ledbetter, 1986) and SS (McCave et al., 2017) and current velocity. Even with the current velocity measured at a variety of locations and the natural complexity inherent in a field site, both studies found that a measure of the average silt size in the deposit was linearly related to the current velocity. For example, the data of Ledbetter (1986) yields a relationship of $d_{ms} = 0.46U + 13.95$ ($R^2 = 0.82$) where d_{ms} is the mean silt size in μm and U is the current velocity in cm/s. Here the slope, 0.46, is only slightly lower than the values obtained with our laboratory study with the intercept falling at the low end of our measured range (Fig. 11). Furthermore, in McCave et al. (2017), slope values from their regression of $SS_{mean} = mU + b$, with SS_{mean} in μm and U in cm/s, ranged from $m = 0.59$ to 0.88 (μm-s/cm) with intercept values between $b = 15.6$ to 7.6 (μm). These slope values from McCave et al. (2017) are all inline with those we obtained in our flume study, with the intercept values being slightly smaller than ours.

The similarity in form of the relationship (linear) and the values of the regression coefficients between our laboratory study and the field suggest at least two cosupporting lines of thought. The first is that the laboratory experiments reasonably reproduced depositional sorting even at their drastically reduced scale. The second, assuming the flume experiments do capture the first-order physics, is that the sorting experienced in the field could be due to depositional sorting with the changes in the slope of the relationship being reflective of the distance from the sediment input or changes in source sediment composition similar to the suggestion by McCave et al. (2017).

To the best of our knowledge, there have been no laboratory studies that have examined the relationship between SS_{mean}, U, and distance from the suspended sediment source. The closest studies to ours have been the studies of Hamm et al. (2009) and Hamm and Dade (2013). Both of these studies examined the dynamics of silt transport in a recirculating racetrack flume. However, only Hamm and Dade (2013) specifically set out to examine how the grain size distribution and SS_{mean} varied with current velocities ranging from 20 to 53 cm/s. For the experiments, they used glass microspheres with diameters in the range of 13 to 44 μm. Similar to our observations, the experiments produced both linear streaks of clustered silt particles moving as bed load and mobile barchan shaped ripples. However, contrary to our findings, the study did not report evidence of grain size sorting within the bedforms as a function of flow velocity.

We suggest that there are at least three differences between our study and that of Hamm and Dade (2013) that likely account for the different outcomes of the two studies with respect to sorting of silt. The first is that the velocities we used are nearly all lower than those of Hamm and Dade (2013). In our experiments velocity ranged from 5 to 25 cm/s compared to the 20 to 53 cm/s used by Hamm and Dade (2013). The velocities used here are more akin to typical bottom current velocities in deep-sea depositional environments. The second major difference is that we used a flow through flume rather than a racetrack flume, which allowed us to examine the role of downstream advective sorting. The third is that we used crushed silica silt and clay mineral as our sediment type instead of glass microspheres. We expect that the first two differences are the most significant in driving the differences in bed texture relationships with current velocity between the two studies.

4.2. Modeling the trends in $SS_{mean} = SS_{mean}(x, U)$

In this section, we explore the ability of the naive model to capture the trends in the experimental data, both in terms of downstream and at-a-station trends, and use the model to consider how changes in the input sediment size distribution can impact $SS_{mean} = SS_{mean}(x, U)$.

4.2.1. *Model comparison with downstream flume data*

If we use the equations for α_i and $E_{s,i}$ suggested by Hamm et al. (2009) (Eqs. 3 and 4), and the Ferguson and Church (2004) settling velocity relation, then the naive depositional model coupled with measured data has no calibration parameters. The inputs for the model include size distribution and inlet concentration (used to define $C_{i,0}$), the flow depth, velocity, and shear velocity, with the resulting output being $f_{b,i} = f_{b,i}(x, U)$ from which SS_{mean} can be calculated. Of the measured inputs, those related to the hydraulics are well constrained with little experimental or measurement variability. Measured silt distributions from a deposit location under identical hydraulic conditions varied little from run to run in our preliminary experiments. Nevertheless, we did observe rather significant variability in the measured size distribution of the silt in the sediment hopper from run to run. Because the depositional model is sensitive to changes in the initial grain size distribution, we elected to compare the model to data from the flume using a synthetic initial SS size distribution. The synthetic distribution was based on an average of the measured values and assumes a normal distribution of log transformed grain sizes (as described in Section 2.2).

Overall, the model captures the general shape of the $SS_{mean} = SS_{mean}(x)$ for a given velocity and the basic trend of the relationship with velocity. However, on the whole, the model does the best at capturing the data for the intermediate velocities (U = 10-20 cm/s). For low velocities (U = 5 cm/s) the model generally predicts a coarser SS_{mean} than the observation, whereas for the higher velocities it tends to underestimate SS_{mean} relative to the experimental data (Fig. 12).

One reason for the underestimation of SS_{mean} at higher velocity might be the size independent nature of α and E_s in the Hamm et al. (2009) formulations and the near zero value of E_s for our particular flow conditions. Rather than being size independent, one might expect E_s to go up as grain size reduces under the consideration that it is easier to entrain smaller particles. This reasoning is common in entrainment functions for sand (e.g., Garcia and Parker, 1991), but it goes against the reasoning and data presented in Hamm et al. (2009) for entrainment of particles smaller than the viscous sublayer thickness. If the erosion and deposition functions did include an element of size dependence,

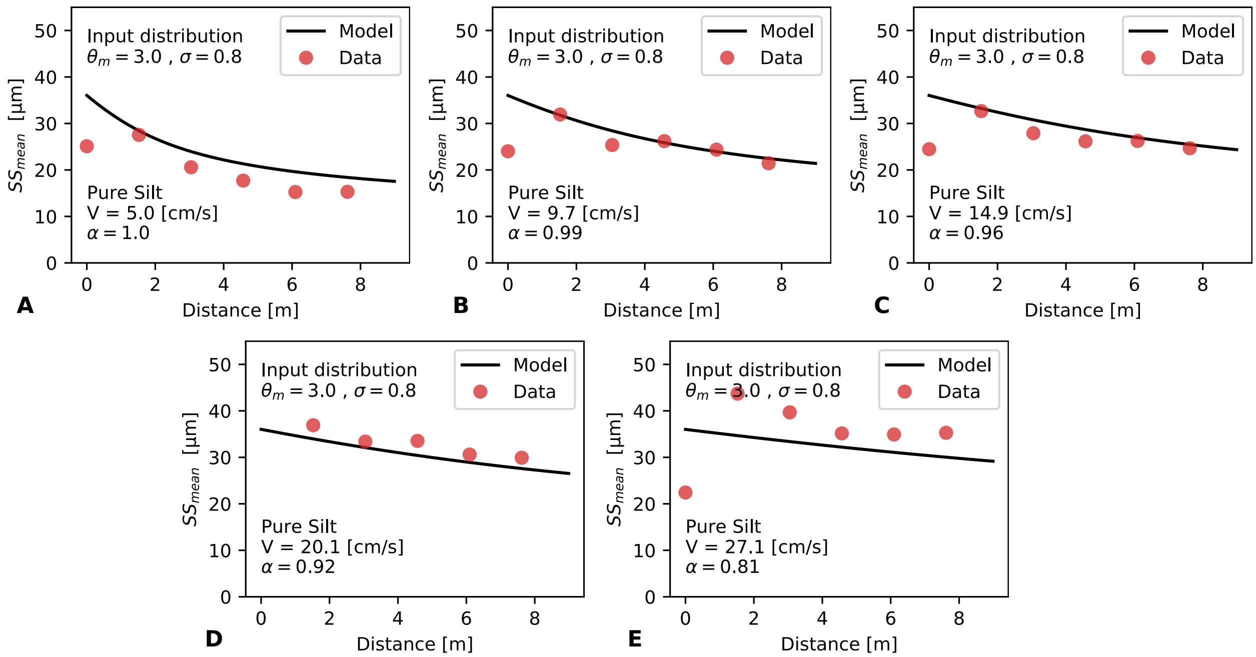

Figure 12: Comparison between the model and observations for low, moderate, and high velocities. SS_{mean} at $x = 0$ m corresponds to the inlet sample SS_{mean}.

finer material would stay in suspension longer at higher flows relative to large particles.

An attempt to improve the model to better match the experimental data was done by introducing the approach of Mooneyham and Strom (2018) to model the erosion and deposition terms (in place of Eqs. 3 and 4). The Mooneyham and Strom (2018) approach is less sophisticated than other deposition and entrainment functions, but it does provide size-class-dependent net deposition and erosion functionality and it was developed for suspensions of clay and silt moving over impermeable and permeable beds. However, even after tuning the coefficients in the model, the method was not able to provide a substantial increase in descriptive power over the model described in Section 2.2 using Equations 3 and 4 for α and E_s.

Through trial and error, it was found that the best match between the flume deposit data and the model was obtained by altering the size distribution of the inlet sediment. Reasonable matches between the data and the model could be obtained by increasing the mean size of the inlet distribution with current velocity. For example, for the pure silt case, using $\theta_m = 2.6$, 2.8, 2.8, 3.2, and 3.5 for the cases of $U = 5$, 10, 15, 20, and 25 cm/s (with $\sigma = 0.8$) yielded a good fit between the model and data. An even better fit could be obtained by also changing σ by up to ± 0.2. Because we have no reason to expect that the inlet size distribution in our experiments was a function of current velocity, we have opted to simply use a single size distribution in the modeling analysis.

4.2.2. At-a-station trends

Similar to our experimental data, our model predicts a general steepening of the $SS_{mean} = SS_{mean}(U)$ relationship (stronger sorting) with an increase in the distance from the flume inlet or source of suspended sediment (Fig. 1B and 11). However, the model predicts a logarithmic form of the relationship rather than a linear one. The discrepancy in the shape of the relationship could be due to at least one of the following two explanations. The first is that it is possible that $SS_{mean} = SS_{mean}(U)$ is truly logarithmic at a given station, but that our experimental data were not able to capture the underlying functionality. That is, given the experimental variability, the limited number of velocities tested, and the near linear shape of the underlying log relations, the data were insufficient to differentiate between a linear and log form. The second possible explanation is that the model is too simplistic and either needs to account for changes in the arrival rate of sediment to the bed or re-entrainment of particles that make it to the bed.

4.2.3. The role of input grain size distribution

Modeling the downstream trends in grain size revealed that the model is strongly dependent on the input grain size distribution, which in natural systems can, in turn, be related to the ultimate source of the sediment. The potential for the relationship between SS_{mean} and current velocity to be dependent on the size distribution of the source sediment has been discussed in the literature (McCave and Hall, 2006). Indeed, McCave et al. (2017) attributed differences in the linear regression coefficients between SS_{mean} and U they observed in different groupings of data to differences in the nature of the input sediment and potentially to differences in the distance from the source.

Here we use the model to examine how changes in grain size distribution of the input material impact the $SS_{mean} = SS_{mean}(U)$ relationship at different downstream distances (Fig. 13). For the analysis we have used our flume data and scale, but the analysis could potentially be applied to field scale conditions. The model confirms that the $SS_{mean} = SS_{mean}(U)$ relationship, in a setting of advective depositional sorting, depends on both the distance from the input and the size distribution of the input sediment. Coarsening of the input and moving up-current so as to be closer to the source both have the effect of producing deposits that are relatively coarser. Coarsening of the input sediment also leads to an increase in the slope of the $SS_{mean} = SS_{mean}(U)$ relationship (stronger sorting) at a given distance from the input.

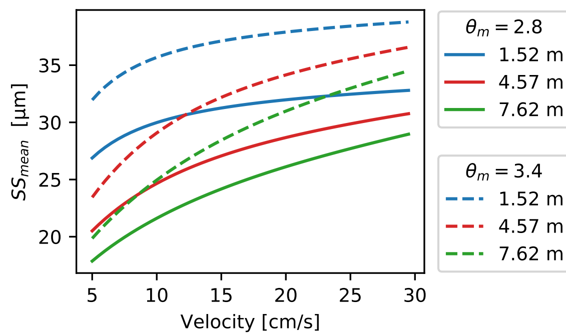

Figure 13: Model output showing the role of input grain size distribution on SS_{mean} trends with distance from input and velocity. Colors represent distance from input. The two different line types represent the two different sediment input distributions. Input 1 (solid lines) is for a distribution with $\theta_m = 2.8$ (16 μm) and input 2 (dashed lines) has $\theta_m = 3.4$ (30 μm); both have $\sigma = 0.8$.

4.3. The role of clay content in the input sediment

One of the goals of these experiments was to examine the influence of clay on the sorting of silt. To do this we ran experiments with pure silt, pure clay mineral, and two different mixtures of silt and clay (Table 1). The presence of clay in the inlet sediment clearly had an influence on the morphology of the bed that developed with time. The higher the percentage of clay, the more suppressed the silty bedforms. It is possible that this suppression of bedforms might have been due to the cohesive nature of the clay (Schindler et al., 2015). It is also possible that bedforms were not as pronounced in beds that developed from the clay-silt mixture relative to those with pure silt because of the overall reduced concentration of silt in input sediment under equivalent inlet concentrations.

While inclusion of clay did change the bed morphology, added clay in the input sediment did not have a strong influence on the sorting properties of the silt. Both downstream and at-a-station trends in $SS_{mean} = SS_{mean}(x, U)$ were relatively insensitive to the amount of clay in the input sediment. This behavior can be seen in Figure 11 and Table 3 where slope and intercept values in the regression of $SS_{mean} = mU + b$ show little variability with the silt to clay ratio. We expect this outcome is a reflection of the little influence the suspended clay has on advective depositional sorting in our experiments.

The presence of clay has the possibility of influencing sorting of silt through two mechanisms. The first would be through binding of clay and silt particles into flocs within the suspension, thereby altering the settling velocity of both fractions (Tran and Strom, 2017). We looked for the occurrence of clay-silt floc binding in suspension and on the bed using the camera system explained in Rouhnia and Strom (2017) and Mooneyham and Strom (2018). In all samples, no indication of binding of the two fractions was evident. The silt existed as independent grains and the clay in visible aggregates roughly the same size as the silt or below the resolution of the camera (≈ 15 μm); no large, low-density flocs such as those in Tran and Strom (2017) were found.

The second way in which clay could have impacted the depositional sorting of silt is through alterations to the deposition and re-entrainment rates (α and E_s in the model). If deposited clay provided a measure of cohesion, it might lead to increased retention of fine silt particles that might have otherwise been resuspended back up into the flow leading to less-well sorted silt. While such a situation seems plausible, our experiments do not support this line of reasoning. There was additional variability in the silt size distribution for the runs with clay, but the overall slope and intercept regression coefficients were very similar regardless of the amount of clay added. This might not have been the case if the clay was depositing to a thick bed of unconsolidated mud rather than an initially starved acrylic flume.

4.4. Bed load

Both the SS hypothesis and our depositional model assume that particles do not move along the bed once they are deposited; i.e., no bed load transport. However, bed load was apparent in all silt and silt-clay experiments at or above $U = 15$ cm/s. It is this bed load that resulted in the creation of ripples that would migrate downstream with or without sediment in suspension. The pure silt ripples that formed in our non recirculating flume closely resembled in size and shape the ripples that formed in race-track flume experiments of Yawar and Schieber (2017) (at 25 cm/s) and Hamm and Dade (2013) (at 20 cm/s). The silt-clay ripples were also similar is size, but contained some clay clumps. Pure clay experiments did not produce bedform similar to those of Schieber et al. (2007). Schieber et al. (2007) found that clay would form floccule ripples at and above velocities tested in these experiments. The implications of this bed load transport is that material does have the ability to transport downstream below a critical shear stress for re-entrainment. This is acknowledged in the SS hypothesis, however is said to be diminished due to biological activity that locks sediment in place.

The implication of bed load transport of deposited grains is that particles that originally deposited at one location under advective sorting could move to another location over long enough periods of time before becoming buried and incorporated into the sedimentary record at a particular location. Although our work did not focus on the effects of bed load transport, such movement could alter the at-a-station relationship between SS_{mean} and U. Furthermore, for cases where bed load is significant, the advective depositional sorting model would need to be updated to include bed load transport.

4.5. Critical conditions

Our experiments show that silt can deposit at velocities of at least 25 cm/s (u_*=1.38 cm/s) with a d_{50} of around 35-40 microns. This value is significantly larger than the critical depositional shear velocity of 0.67 cm/s suggested in McCave et al. (2017), but is inline with the results of Hamm and Dade (2013) who saw silt deposit into barchan ripples at velocities up to 30 cm/s (0.28 Pa). Yawar and Schieber (2017) also observed barchan ripples form from silt at velocities of up to 55 cm/s (material D_{50} of 50 microns), and 40 cm/s (material D_{50} of 30 microns). Based on these values, it seems reasonable to expect that silt can actively deposit to the ocean floor under the majority of boundary current conditions.

Deposition of clay on its own seems to achieve a critical velocity between 20 and 25 cm/s (0.13 - 0.19 Pa), although the inclusion of silt appears to increase this point, potentially due to low energy areas around silt bedforms. McCave et al. (1995) cites a critical shear velocity measured in a radial laminar flow cell for particles with a diameter on 10 microns to be 0.32 cm/s. The critical shear velocity and shear stress for the deposition and accumulation of clay in our experiments was around $u_* = 1.12$ cm/s and $\tau_B = 0.13$ Pa, much higher than those used in the SS hypothesis. Clay deposition thresholds from our experiments are inline with those of Schieber et al. (2007) and Yawar and Schieber (2017) where it was found that floccule ripples can form at velocities ranging from 10-26 cm/s. These high critical conditions for silt and clay deposition, and the consolidating effect of deposited clay, could lead one to conclude that only under extreme events (e.g., benthic storms; Gardner et al., 2017) does erosion occur. In between such episodic events, contour currents likely function as a depositional system and advectively sort material eroded in storms.

5. Conclusions

In this study we used a laboratory experiment to investigate the relationship between the mean sortable silt, SS_{mean} and average current velocity over ranges that are typical of deep-sea environments (U = 5-25 cm/s). The relationship between these two variables was examined both at a particular distance from the input of suspended sediment (at a station) and as a function of total distance from the sediment input (downstream). Sediment used in the experiments consisted of crushed silica sand in the silt size range and different mixtures of the silica silt with clay minerals. The combination of the experimental methods and materials led to advective depositional sorting where silt sizes in the deposit fine with distance from the input and coarsen with increasing velocity and current thickness.

We found that at a particular location in the flume, SS_{mean} was linearly related to U similar to the field calibration of McCave et al. (2017) regardless of clay content in the source sediment. Linear regression between SS_{mean} in microns and U in cm/s produced fits with R^2 values between 0.7 and 0.94 and coefficient values similar to those from the field, even though the scales of the two studies are very different. In general, the slope of the $SS_{mean} = SS_{mean}(U)$ regression increased, while the intercept decreased, with distance from the input in both the theory and experiments.

A model for SS_{mean} in the deposit was developed using simple theory. For the experimental conditions, the model was able to reasonably describe the size distribution of silt in the deposit as a function of the input grain size distribution, the distance from the input, velocity, and current thickness. The model predicted the downstream fining and the change in the slope of the $SS_{mean} = SS_{mean}(U)$ relationship with distance from the input. However, the model was not able to strictly demonstrate the linear relationship in $SS_{mean} = SS_{mean}(U)$ at a particular station found in the experiments. The model was also used to show what types of impact a change in sediment source might have on the $SS_{mean} = SS_{mean}(U)$ relations.

Both the experiments and model demonstrated the importance of the thickness of the current, h, in the sorting process. More specifically, the model shows that the amount of silt in size fraction, i, within a deposit is strongly dependent on the ratio x/L_i; where x is the distance from the source and L_i is the advective length scale $L_i = hU/(\alpha w_{s,i})$. This shows that that L_i is linearly dependent on both U and h. Doubling either will produce a doubling of L_i.

This study shows that silt can advectively sort under depositional conditions, and it highlights how the distance from the input, flow thickness, and changes in the input grain size can alter the relationship. The similarity in the linearity between SS_{mean} and U and the regressed slope and intercept values between the laboratory and field suggest that the field data of McCave et al. (2017) was also advectively sorted.

Acknowledgments

Funding for this work was provided by American Chemical Society-Petroleum Research Fund-New Directions grant 57811-ND awarded to BWR and KS. Data associated with this study can be obtained from GitHub at github.com/FluidSedDynamics, or by contacting the corresponding author (strom@vt.edu).

References

Bianchi, G. G., Hall, I. R., McCave, I. N., and Joseph, L. (1999). Measurement of the sortable silt current speed proxy using the sedigraph 5100 and coulter multisizer iie: precision and accuracy. *Sedimentology*, 46(6):1001–1014.

Broecker, W. S., Peacock, S. L., Walker, S., Weiss, R., Fahrbach, E., Schroeder, M., Mikolajewicz, U., Heinze, C., Key, R., Peng, T.-H., and Rubin, S. (1998). How much deep water is formed in the southern ocean? *Journal of Geophysical Research: Oceans*, 103(C8):15833–15843.

Dixit, J. G., Mehta, A. J., and Partheniades, E. (1982). Redepositional properties of cohesive sediments deposited in a long flume. Report UFL/COEL-82/002, Coastal & Oceanographic Engineering Department, University of Florida, Gainesville, FL USA.

Einstein, H. A. and Krone, R. B. (1962). Experiments to determine modes of cohesive sediment transport in salt water. *Journal of Geophysical Research*, 67(4):1451–1461.

Ferguson, R. and Church, M. (2004). A simple universal equation for grain settling velocity. *Journal of Sedimentary Research*, 74(6):933–937.

Garcia, M. and Parker, G. (1991). Entrainment of bed sediment into suspension. *Journal of Hydraulic Engineering*, 117(4):414–435.

García, M. H. (2008). *Sediment Transport and Morphodynamics. Sedimentation Engineering*, chapter 2 Sediment Transport and Morphodynamics, pages 21–163. ASCE Manuals and Reports on Engineering Practice No. 110. ASCE.

Gardner, W. D., Tucholke, B. E., Richardson, M. J., and Biscaye, P. E. (2017). Benthic storms, nepheloid layers, and linkage with upper ocean dynamics in the western north atlantic. *Marine Geology*, 385:304 – 327.

Hamm, N. T. and Dade, W. B. (2013). A laboratory study of dynamic sorting of fine, non-cohesive particles by steady, unidirectional currents. *Marine Geology*, 336:215 – 222.

Hamm, N. T., Dade, W. B., and Renshaw, C. E. (2009). Fine particle deposition to initially starved, stationary, planar beds. *Sedimentology*, 56(7):1976–1991.

Haralampides, K., McCorquodale, J. A., and Krishnappan, B. G. (2003). Deposition properties of fine sediment. *Journal of Hydraulic Engineering*, 129(3):230–234.

Heezen, B. C., Hollister, C. D., and Ruddiman, W. F. (1966). Shaping of the continental rise by deep geostrophic contour currents. *Science*, 152(3721):502–508.

Jarvie, D. M., Hill, R. J., Ruble, T. E., and Pollastro, R. M. (2007). Unconventional shale-gas systems: The Mississippian Barnett Shale of north-central Texas as one model for thermogenic shale-gas assessment. *AAPG Bulletin*, 91(4):475–499.

Kleiven, H. K. F., Hall, I., McCave, I., Knorr, G., and Jansen, E. (2011). Coupled deep-water flow and climate variability in the middle Pleistocene North Atlantic. *Geology*, 39(4):343–346.

Knutz, P. (2008). Paleoceanographic significance of contourite drifts. *Developments in Sedimentology*, 60:511–535.

Lau, Y. L. and Krishnappan, B. G. (1992). Size distribution and settling velocity of cohesive sediments during settling. *Journal of Hydraulic Research*, 30(5):673–684.

Law, B., Hill, P., Milligan, T., Curran, K., Wiberg, P., and Wheatcroft, R. (2008). Size sorting of fine-grained sediments during erosion: Results from the western gulf of lions. *Continental Shelf Research*, 28(15):1935 – 1946.

Ledbetter, M. T. (1986). A late pleistocene time-series of bottom-current speed in the vema channel. *Palaeogeography, Palaeoclimatology, Palaeoecology*, 53(1):97 – 105.

McCave, I. and Andrews, J. (2019). Distinguishing current effects in sediments delivered to the ocean by ice. i. principles, methods and examples. *Quaternary Science Reviews*, 212:92 – 107.

McCave, I., Thornalley, D., and Hall, I. (2017). Relation of sortable silt grain-size to deep-sea current speeds: Calibration of the 'mud current meter'. *Deep Sea Research Part I: Oceanographic Research Papers*, 127(Supplement C):1 – 12.

McCave, I. N. and Hall, I. R. (2006). Size sorting in marine muds: Processes, pitfalls, and prospects for paleoflow-speed proxies. *Geochemistry, Geophysics, Geosystems*, 7(10):n/a–n/a.

McCave, I. N., Manighetti, B., and Robinson, S. G. (1995). Sortable silt and fine sediment size/composition slicing: Parameters for palaeocurrent speed and palaeoceanography. *Paleoceanography*, 10(3):593–610.

Mooneyham, C. and Strom, K. (2018). Deposition of suspended clay to open and sand-filled framework gravel beds in a laboratory flume. *Water Resources Research*, 54:323–344.

Niño, Y., Lopez, F., and Garcia, M. (2003). Threshold for particle entrainment into suspension. *Sedimentology*, 50(2):247–263.

Partheniades, E. (2006). *Engineering Properties and Hydraulic Behavior of Cohesive Sediments*. CRC Press.

Rebesco, M., Hernández-Molina, F. J., Rooij, D. V., and Wåhlin, A. (2014). Contourites and associated sediments controlled by deep-water circulation processes: State-of-the-art and future considerations. *Marine Geology*, 352:111 – 154.

Richardson, M. J., Weatherly, G. L., and Gardner, W. D. (1993). Benthic storms in the argentine basin. *Deep Sea Research Part II: Topical Studies in Oceanography*, 40(4):975 – 987.

Rouhnia, M. and Strom, K. (2017). Sedimentation from buoyant muddy plumes in the presence of interface mixing: An experimental study. *Journal of Geophysical Research: Oceans*, 122:2652–2670.

Saffman, P. G. (1965). The lift on a small sphere in a slow shear flow. *Journal of Fluid Mechanics*, 22:385–400.

Schieber, J. (1998). Sedimentary features indicating erosion, condensation, and hiatuses in the chattanooga shale of central tennessee: relevance for sedimentary and stratigraphic evolution. In Schieber, J., Zimmerle, W., and Sethi, P., editors, *Shales and Mudstones, Basin Studies, Sedimentology and Paleontology*, pages 187–215. Schweizerbart'sche Verlagsbuchhandlung, Stuttgart.

Schieber, J. (2011). Reverse engineering mother nature – shale sedimentology from an experimental perspective. *Sedimentary Geology*, 238(1-2):1 – 22.

Schieber, J., Southard, J. B., and Thaisen, K. (2007). Accretion of mudstone beds from migrating floccule ripples. *Science*, 318:1760–1763.

Schindler, R. J., Parsons, D. R., Ye, L., Hope, J. A., Baas, J. H., Peakall, J., Manning, A. J., Aspden, R. J., Malarkey, J., Simmons, S., Paterson, D. M., Lichtman, I. D., Davies, A. G., Thorne, P. D., and Bass, S. J. (2015). Sticky stuff: Redefining bedform prediction in modern and ancient environments. *Geology*, 43(5):399–402.

Slatt, R. M. (2011). Important geological properties of unconventional resource shales,. *Open Geosciences*, 3(4):435–448.

Teeter, A. M. (1997). Size-dependant erosion of two silty-clay sediment mixtures. resreport, Waterways Experiment Station, Vicksburg, MS, USA.

Thornalley, D. J. R., Blaschek, M., Davies, F. J., Praetorius, S., Oppo, D. W., McManus, J. F., Hall, I. R., Kleiven, H., Renssen, H., and McCave, I. N. (2013). Long-term variations in iceland–scotland overflow strength during the holocene. *Climate of the Past*, 9(5):2073–2084.

Tran, D. and Strom, K. (2017). Suspended clays and silts: Are they independent or dependent fractions when it comes to settling in a turbulent suspension? *Continental Shelf Research*, 138:81 – 94.

Yawar, Z. and Schieber, J. (2017). On the origin of silt laminae in laminated shales. *Sedimentary Geology*, 360(Supplement C):22–34.